Available online at www.sciencedirect.com
ScienceDirect
Tectonophysics 425 (2006) 83–99
TECTONOPHYSICS
www.elsevier.com/locate/tecto

On the role of heat flow, lithosphere thickness and lithosphere density on gravitational potential stresses

Christophe Pascal *

Faculty of Earth and Life Sciences, Vrije Universiteit, De Boelelaan 1085, 1081 HV Amsterdam, The Netherlands

Received 9 March 2006; received in revised form 22 June 2006; accepted 12 July 2006
Available online 1 September 2006

Abstract

Gravitational potential stresses (GPSt) are known to play a first-order role in the state of stress of the Earth's lithosphere. Previous studies focussed mainly on crust elevation and structure and little attention has been paid to modelling GPSt using realistic lithospheric structures. The aim of the present contribution is to quantify gravitational potential energies and stresses associated with stable lithospheric domains. In order to model realistic lithosphere structures, a wide variety of data are considered: surface heat flow, chemical depletion of mantle lithosphere, crustal thickness and elevation. A numerical method is presented which involves classical steady-state heat equations to derive lithosphere thickness, geotherm and density distribution, but additionally requires the studied lithosphere to be isostatically compensated at its base. The impact of varying surface and crustal heat flow, topography, Moho depth and crust density on the signs and magnitudes of predicted GPSt is systematically explored. In clear contrast with what is assumed in most previous studies, modelling results show that the density structure of the mantle lithosphere has a significant impact on the value of the predicted GPSt, in particular in the case of thick lithospheres. Using independent information from the literature, the method was applied to get insights in the state of stress of continental domains with contrasting tectono-thermal ages. The modelling results suggest that in the absence of tectonic stresses Phanerozoic and Proterozoic lithospheres are spontaneously submitted to compression whereas Archean lithospheres are in a neutral to slightly tensile stress state. These findings are in general in good agreement with global stress measurements and observed geoid undulations.

Keywords: Potential energy; Geotherm; Lithosphere buoyancy; Chemical depletion; Geoid

1. Introduction

Gravitational potential energy and subsequent gravitational potential stresses are the direct consequence of lateral density heterogeneities existing both at lithospheric (e.g. Artyushkov, 1973; Fleitout and Froidevaux, 1982) and sublithospheric (e.g. Lithgow-Bertelloni and Guynn, 2004) levels. The influence of gravitational potential energy on the state of stress of the Earth's lithosphere is nowadays widely acknowledged. This concept has been successful in explaining first-order (e.g. ridge-push, Dahlen, 1981) and second-order stress patterns (e.g. gravitational collapse of elevated landmasses, England and Houseman, 1989) documented on the World Stress Map (Fig. 1, Reinecker et al., 2005), as well as in explaining intraplate seismicity in North America (Thybo et al., 2000). Although the concept has often been used to predict the state of stress of the lithosphere (e.g.

* Present address: NGU, Geological Survey of Norway, N-7491 Trondheim, Norway. Fax: +47 73904494.
E-mail address: christophe.pascal@ngu.no.

0040-1951/$ - see front matter © 2006 Elsevier B.V. All rights reserved.
doi:10.1016/j.tecto.2006.07.012

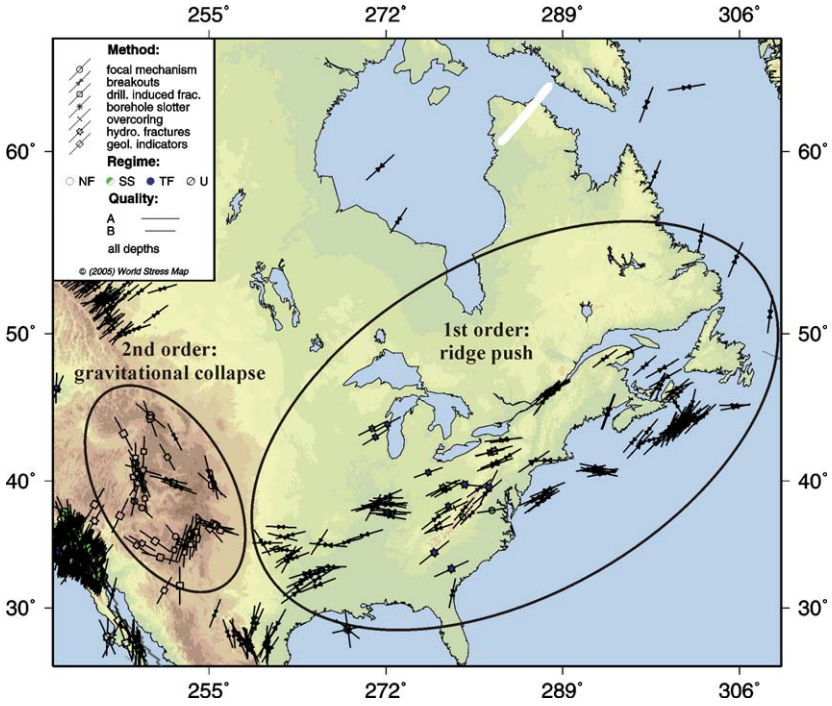

Fig. 1. Example of 1st and 2nd order stress patterns (i.e. ridge push and gravitational collapse stresses respectively) induced by lateral variations in gravitational potential energy in the Earth's lithosphere. After Reinecker et al. (2005).

Artyushkov, 1973; Fleitout and Froidevaux, 1982, 1983; Coblentz et al., 1994; Jones et al., 1996; Zoback and Mooney, 2003), previous works focused mainly on surface and/or Moho topographies and used simplified thermal and density structures for mantle lithosphere. Examples are the use of constant mantle lithosphere densities (Artyushkov, 1973; Fleitout and Froidevaux, 1982, 1983), no base lithosphere topography (Coblentz et al., 1994), an empirical mantle lithosphere density distribution (Jones et al., 1996) and a linear geotherm (Zoback and Mooney, 2003). The goal of the present study is to quantify the magnitude of potential stresses affecting lithospheres in isostatic and thermal equilibrium, using realistic ranges for mantle lithosphere reference densities (e.g. Poudjom Djomani et al., 2001) and for surface heat flow values (e.g. Pollack and Chapman, 1977, Artemieva and Mooney, 2001), and paying attention to petrophysical properties of mantle peridotites derived from laboratory experiments (Guyot et al., 1996; Poudjom Djomani et al., 2001). The present contribution focuses on thermally stable lithospheric domains with typical dimensions exceeding various hundreds of kilometers (i.e. most of the Earth's lithosphere) and, therefore, supported by local isostasy. Lithospheric domains under active tectonic deformation are not considered here and will be treated in a future study. Firstly a numerical method, coupling local isostasy with steady-state heat equations, is introduced. The impact of varying surface and crustal heat flow, topography, Moho depth and average crust density on potential stresses is shown in the following section. Finally, using independent constraints from the literature on surface heat flow, chemical depletion of mantle lithosphere, average topography and crustal thickness, the method is applied to lithospheres with distinct tectono-thermal ages. Modelling results are discussed and confronted to global stress measurements and geoid anomalies.

2. Mathematical formulation

2.1. Coupling steady-state thermal equations and isostatic compensation

In this section, a method is presented to compute lithospheric gravitational potential energy (hereafter GPE) and gravitational potential stresses (hereafter GPSt), taking into account lithosphere structure and elevation and lithosphere density distribution through depth. Compared to more sophisticated numerical methods (e.g. finite elements), the method presents two main advantages: computations are fast and the results are easy to interpret. Mantle lithosphere density depends primarily on the lithosphere geotherm and on chemical depletion of mantle lithosphere with respect to 'fertile' asthenosphere (e.g.

Jordan, 1988; Boyd, 1989). Also, the thermal state of the lithosphere controls its thermal thickness. A steady-state lithospheric thermal regime described by the conductive heat equation (e.g. Pollack and Chapman, 1977; Chapman, 1986) is assumed. The general form of the 1D conductive heat equation is written:

$$\frac{\partial^2 T_L(z)}{\partial z^2} = -\frac{A}{k} \tag{1}$$

where $T_L(z)$ is lithosphere temperature through depth, depth is positive downwards and $z=0$ at the surface, A is heat generation by radioactive decay and k is conductivity. Eq. (1) is integrated with the following boundary conditions:

$$T_L(0) = 0 \tag{2}$$

$$q_S = -k\frac{\partial T_L(z)}{\partial z} \tag{3}$$

where q_S is heat flow measured at the surface. Contrasting heat generations and conductivities are assumed between crust and mantle lithosphere (Fig. 2 Table 1). It is also assumed that crustal radioactive elements are mainly concentrated at shallow depths inside a layer of characteristic thickness D. The remaining crust below this layer has lower heat production (i.e. one order less than the shallow heat-producing layer, Chapman, 1986; Artemieva and Mooney, 2001). The depth of the base of the lithosphere, z_{bl}, is defined by the temperature value $T_{bl} \sim 1300$ °C characterizing Moho temperatures below mid-oceanic ridges. In the present computations z_{bl} is constrained to lie between Moho depth and the olivine–spinel phase transition at 410 km depth (see also Rudnick et al., 1998). This latter maximum depth has to be considered as an end-member value that will be used in the synthetic models presented in the third section of this paper.

The asthenosphere is assumed to be in an adiabatic thermal state:

$$T_A(z) = T_p + Fz \tag{4}$$

The thermal equations and isostatic compensation are coupled using the pressure and temperature dependence of mantle density (Fig. 2). Crust composition is relatively heterogeneous and its density is more dependent on SiO_2 content than on P–T conditions (e.g. Christensen and Mooney, 1995). For the sake of simplicity, crustal density is therefore assumed constant. After integrating the thermodynamic state equation appropriate to conductive media

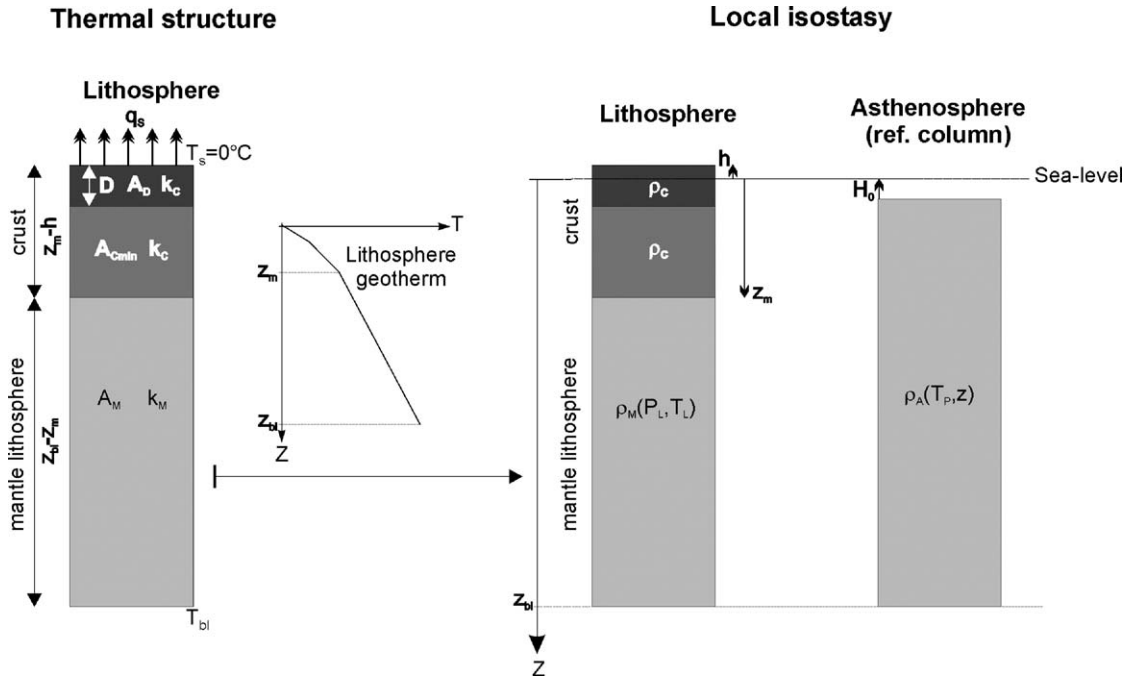

Fig. 2. Model set-up. The computed lithosphere geotherm is used to determine the depth to the base of the lithosphere and the density distribution within the mantle lithosphere. Following Lachenbruch and Morgan (1990), local isostasy at the base of the lithosphere is assumed. See text and Table 1 for symbols.

Table 1
List of parameters used in this study

Quantity	Symbol	Value	Reference
Elevation	h	Variable	
Mid-oceanic ridge depth	h_R	2500 m	Parsons and Sclater (1977)
Oceanic crust thickness	t_{OC}	7000 m	Hager (1983)
Moho depth	z_m	Variable	
Base lithosphere depth	z_{bl}	Computed	
Surface temperature	T_S	0 °C	Artemieva and Mooney (2001)
Surface heat flow	q_S	Variable	
Characteristic thickness	D	10 km	Artemieva and Mooney (2001)
Max. crustal heat production	A_D	Computed	
Heat flow ratio	R_q	Computed	
Min. crustal heat production	A_{cmin}	0.3 μW/m^3	Artemieva and Mooney (2001)
Crust thermal conductivity	k_C	2 W/m/K	–
Water density	ρ_w	1030 kg/m^3	Turcotte and Schubert (2002)
Continental crust density	ρ_C	2830 kg/m^3	Christensen and Mooney (1995)
Oceanic crust density	ρ_{OC}	2850 kg/m^3	This study
Base lithosphere temperature	T_{bl}	1300 °C	This study
Mantle lithosphere heat production	A_M	0.01 μW/m^3	Rudnick et al. (1998)
Mantle lithosphere thermal conductivity	k_M	4 W/m/K	Artemieva and Mooney (2001)
Thermal expansion	α	Temp.-dependent K^{-1}	
Thermal expansion parameter	a	$2.7\cdot10^{-5}$ K^{-1}	Poudjom Djomani et al. (2001)
Thermal expansion parameter	b	10^{-8} K^{-2}	–
Thermal expansion parameter	c	0.12 K	–
Mantle lithosphere compressibility	β_L	7.64 GPa^{-1}	–
Mantle lithosphere ref. density	ρ_{MRef}	Computed	
Buoyant height of sea level	H_0	2500 m	This study
Asthenosphere potential temperature	T_P	1300 °C	Turcotte and Schubert (2002)
Mantle adiabat	F	0.5 °C/km	–
Asthenosphere compressibility	β_A	6.651 GPa^{-1}	Dziewonski and Anderson (1981)
Asthenosphere ref. density	ρ_{ARef}	3390 kg/m^3	Ringwood (1975)
Acceleration of gravity	g	10 m/s^2	Turcotte and Schubert (2002)
Gravitational constant	G	$6.67\cdot10^{-11}$ N m^2/kg^2	–

(e.g. Turcotte and Schubert, 2002), mantle lithosphere density as a function of depth is computed using:

$$\rho_M(z) = \rho_{MRef}(1-\alpha T_L(z) + \beta_L P_L(z)) \quad (5)$$

where ρ_{MRef} is mantle lithosphere reference density (i.e. at P–T standard conditions), α is the volumetric coefficient of expansion, and β_L is isothermal compressibility. α depends on temperature following:

$$\alpha = a + b\ T_L(z) + c(T_L(z))^{-2} \quad (6)$$

a, b and c are experimentally determined parameters (e.g. Guyot et al., 1996; Poudjom Djomani et al., 2001) that are weakly dependent on composition (Poudjom Djomani et al., 2001). Averaged values from Poudjom Djomani et al. (2001) are used here (Table 1).

Because mantle asthenosphere is seen as an adiabatic convecting fluid, derivation of the thermodynamic equations of state leads to a different equation linking density to P–T conditions (Turcotte and Schubert, 2002):

$$\rho_A(z) = \rho_{AP=0}/(1-\rho_{AP=0} g \beta_A z) \quad (7)$$

where g is gravity acceleration, β_A is adiabatic compressibility and

$$\rho_{AP=0} = \rho_{ARef}(1-\alpha_{T_P} T_P) \quad (8)$$

where α_{T_P} is computed using Eq. (6) for $z=0$.

Isostatic compensation is computed following Lachenbruch and Morgan (1990). Local isostasy as well as 1D thermal models remain acceptable assumptions when studying domains with typical dimensions exceeding various hundreds of kilometers (Turcotte and Schubert, 2002). The approach assumes local isostatic equilibrium between the studied lithosphere column and an ideal reference asthenosphere column (Fig. 2). The depth below sea level of the asthenosphere reference column (i.e. H_0), or conversely the buoyant height of sea

level, is calculated considering asthenosphere density and crust thickness, density and elevation at 'standard' mid-oceanic ridges (Turcotte et al., 1977; Lachenbruch and Morgan, 1990). In order to remain consistent with the parameter values used here (Table 1), H_0 is assigned a value of 2500 m. This value does not differ significantly from that proposed by Lachenbruch and Morgan (1990) (i.e. 2400 m).

The condition for local isostasy at base lithosphere depth is:

$$P_{\mathrm{L}}(z_{\mathrm{bl}}) = P_{\mathrm{A}}(z_{\mathrm{bl}}) \tag{9}$$

where the second term of Eq. (9) represents the pressure of the asthenosphere column at depth z_{bl}.

In detail, pressure at the base of the lithosphere is computed through:

$$P_{\mathrm{L}}(z_{\mathrm{bl}}) = f(h)\int_0^h \rho_{\mathrm{W}} g\,\mathrm{d}z + \int_h^{z_{\mathrm{m}}} \rho_{\mathrm{C}} g\,\mathrm{d}z + \int_{z_{\mathrm{m}}}^{z_{\mathrm{bl}}} \rho_{\mathrm{M}}(z) g\,\mathrm{d}z \tag{10}$$

where $f(h)=0$ if the crust surface is at or above sea level (i.e. $h \leq 0$) and $f(h)=1$ otherwise (i.e. $h>0$). The pressure exerted by the asthenosphere reference column at depth z_{bl} is given by:

$$P_{\mathrm{A}}(z_{\mathrm{bl}}) = \int_{H_0}^{z_{\mathrm{bl}}} \rho_{\mathrm{A}}(z) g\,\mathrm{d}z \tag{11}$$

Depth-dependent (i.e. P–T-dependent) terms in (10) and (11) are computed using (5) and (7) respectively.

The thermal state of the lithosphere, and consequently lithosphere mantle density, is strongly dependent on measured surface heat flow and the ratio between heat flow produced in the 'D layer' (Fig. 2) and surface heat flow:

$$R_{\mathrm{q}} = DA_{\mathrm{D}}/q_{\mathrm{S}} \tag{12}$$

These two critical parameters (i.e. q_{S} and R_{q}) are systematically explored here and a collection of possible lithosphere geotherms is numerically computed (Fig. 3). For each computed geotherm, the condition for local isostasy is tested against the condition that the reference density for mantle lithosphere ranges between 3300 and 3390 kg/m^3. In other words, it is assumed that mantle lithosphere can be depleted with respect to 'primitive' mantle asthenosphere (i.e. pyrolyte, Ringwood, 1975) from 0 to ~2.65%. This range of values encompasses most determinations for the reference density of mantle lithosphere, based on petrologic studies of mantle xenoliths (e.g. Boyd and McCallister, 1976; Jordan, 1988; Boyd, 1989; Boyd et al., 1999; Poudjom Djomani et al., 2001; James et al., 2004). Although denser constituents can be present in the lithosphere (i.e. eclogites), petrological studies suggest that they represent less than 1% of the volume of mantle lithosphere (Schulze, 1989). The procedure described above allows for numerically excluding lithosphere geotherms that imply that corresponding lithospheres are not in isostatic equilibrium, when reasonable values for mantle reference density are considered (Fig. 3). In turn, base lithosphere depth being also limited between Moho and 410 km depth, the initial collection of possible geotherms is also constrained to remain within reasonable limits.

2.2. Computing gravitational potential energy and stresses

Once the thermal structure, the thickness and the density structure of the lithosphere are determined, it is possible to compute GPE and subsequent GPSt for this lithospheric column. Gravitational potential stresses are due to contrasting density distributions between the studied lithosphere column and a given reference column (e.g. Artyushkov, 1973; Fleitout and Froidevaux, 1982).

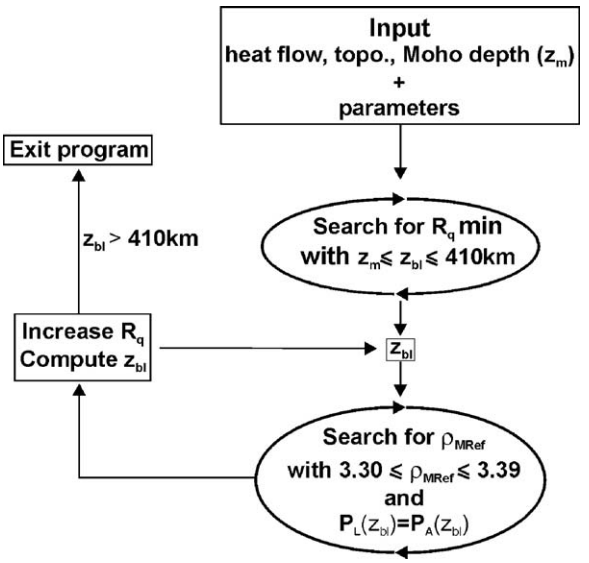

Fig. 3. Simplified program flow chart. The first program loop determines minimum R_{q} values that are in agreement with base of lithosphere depths between Moho depth and the olivine–spinel phase transition depth (i.e. 410 km). In the second loop, the program searches for reference density values for the mantle lithosphere within a reasonable range of values (see text) and accounting for local isostasy. See text and Table 1 for symbols.

Potential stresses are written as a function of lithospheric thickness and the difference in gravitational potential energy (ΔGPE) between the two columns:

$$\mathrm{GPSt} = \sigma_{xx} = \frac{\Delta\mathrm{GPE}}{h - z_{\mathrm{bl}}} \tag{13}$$

ΔGPE is linked to the respective density distributions inside the two columns through:

$$\Delta\mathrm{GPE} = \int_{\mathrm{h}}^{z_{\mathrm{bl}}} (\sigma_{zz}(z) - \sigma_{zz}^{R}(z))\mathrm{d}z \tag{14}$$

where lithostatic pressures for the studied lithospheric column and the reference column are respectively given by:

$$\sigma_{zz}(z) = gf(h)\int_0^h \rho_{\mathrm{W}}\mathrm{d}l + g\int_h^z \rho_{\mathrm{L}}(l)\mathrm{d}l \tag{15}$$

and

$$\sigma_{zz}^{\mathrm{R}}(z) = g\int_{h^{\mathrm{R}}}^z \rho^{\mathrm{R}}(l)\mathrm{d}l \tag{16}$$

To compare the predicted differences in potential energy to observed geoid undulations the following equation will be used (Turcotte and Schubert, 2002):

$$\Delta N = \frac{2\pi G}{g^2}\Delta\mathrm{GPE} \tag{17}$$

The reference column is assumed to be in a zero stress state in the absence of tectonic forces. Its choice is critical because it directly influences the magnitude and the sign of the predicted stresses. A 'standard' mid-oceanic ridge was traditionally proposed as reference column (e.g. England and Houseman, 1989). However, as pointed out by Coblentz et al. (1994) this choice is contradictive with the obvious role played by body forces in the mechanism of spreading of mid-oceanic ridges (Dahlen, 1981). In the present study, the asthenosphere reference column used to compute isostasy is selected as reference column to compute potential stresses also (Fig. 2). The reference column used in this study is similar to the one selected by Jones et al. (1996) and Zoback and Mooney (2003). But in contrast with these previous studies more attention is paid here to model realistic thermal and density structures for the lithosphere. It will be shown in the following section that the reference column chosen in the present study results in realistic stress signs and magnitudes.

3. Interplay between heat flow, topography, Moho topography and crustal density

Using the method described above it becomes possible to jointly compute the lithospheric geotherm, mantle density structure and gravitational potential energy and stresses. The prime objective of this section is to show how ΔGPE and GPSt for a thermally relaxed continental lithosphere relate to surface heat flow, elevation, and crustal thickness and density.

3.1. Impact of surface heat flow on ΔGPE and GPSt

Fig. 4 shows the values computed for the depth of the base of the lithosphere, mantle density depletion, ΔGPE and GPSt, as a function of surface heat flow and the ratio between crustal heat flow from shallow sources (i.e. from the 'D-layer', Fig. 2) and surface heat flow, for a 35-km-thick continental crust at sea level. This crustal thickness represents an average thickness between the different types of continental crust and not the average thickness of continental crust, which is dominated by a large proportion of shields and platforms (Christensen and Mooney, 1995; Mooney et al., 1998). A wide range of R_{q} values (see Eq. (12)) between 25% and 75% was explored. Higher values result in unreasonably thick lithospheres (i.e. $z_{\mathrm{bl}} > 180$ km) for surface heat flow higher than 70 mW/m^2, and lower values lead to excessively low heat generation values for the 'D-layer' (i.e. $A_{\mathrm{D}} < 1$ μW/m^3). Typical continental heat flow values in between 30 and 90 mW/m^2 were considered (Chapman, 1986), where the lowest values (i.e. $q_{\mathrm{S}} < 60$ mW/m^2) are traditionally associated with Precambrian lithosphere (e.g. Balling, 1995; Kukkonen and Peltonen, 1999; Artemieva and Mooney, 2001).

The solution domains presented in Fig. 4 are also limited according to the assumptions made in the previous section. Upper left boundaries reflect the assumed maximum depth for the base of the lithosphere (i.e. $z_{\mathrm{bl}} = 410$ km) as shown in Fig. 4a, whereas lower right boundaries are imposed by the maximum reference density value allowed for mantle lithosphere (i.e. $\rho_{\mathrm{MRef}} = \rho_{\mathrm{ARef}} = 3390$ kg/m^3 or $\Delta\rho = 0$, Fig. 4b). As a consequence, lithosphere thickness less than ~130 km are excluded from the domain of possible solutions (Fig. 4a) and minimum lithosphere thickness values are here associated with chemically undepleted lithospheric mantle (i.e. $\Delta\rho \sim 0$, Fig. 4b). It is equivalent to say that lithosphere thinner than 130 km cannot be in isostatic equilibrium for the parameters selected here and for mantle reference densities lower or equal to the reference density of the asthenosphere. It is also interesting to note that, in the context of thermally relaxed lithosphere, relatively high

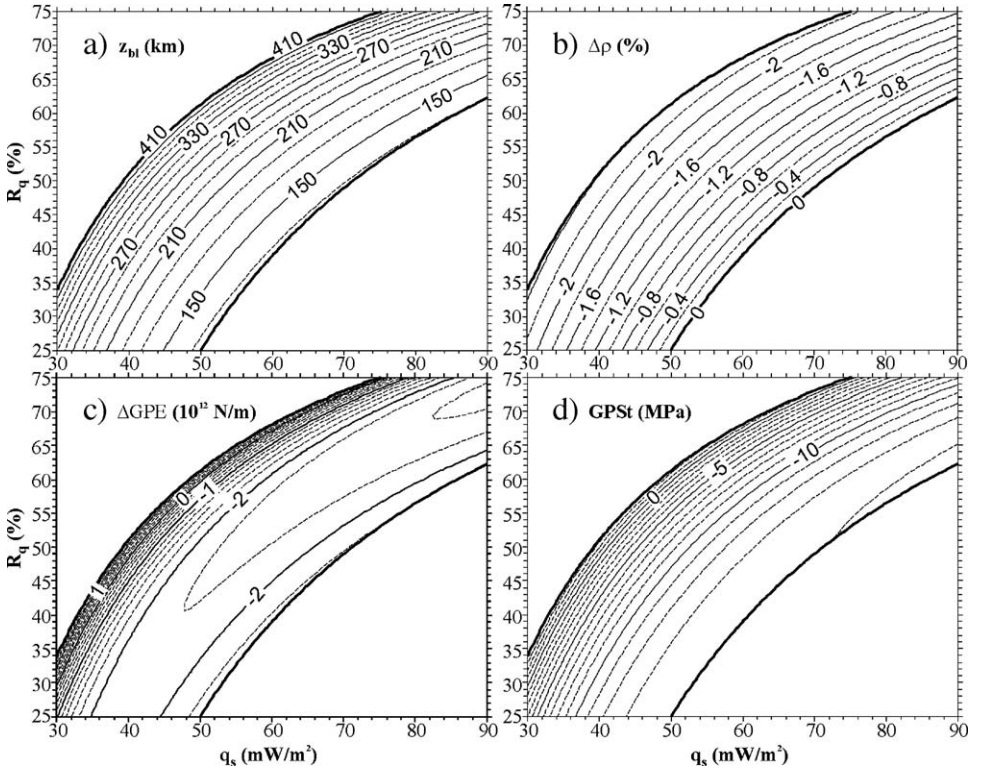

Fig. 4. Computed (a) base lithosphere depths (z_{bl}), (b) density depletion of mantle lithosphere with respect to asthenosphere ($\Delta\rho$), (c) ΔGPE and (d) GPSt as a function of surface heat flow (q_S) and R_q. The crust is assumed to be 35 km thick and its surface at sea level. Parameter values are given in Table 1.

surface heat flow values (i.e. $q_S > 75$ mW/m^2) are possible only if the proportion of heat coming from the 'D-layer' exceeds $R_q = 50\%$ (Fig. 4). We also note that the degree of depletion for mantle lithosphere reference density correlates positively with surface heat flow and negatively with lithosphere thickness in good agreement with previous studies (e.g. Jordan, 1988; Poudjom Djomani et al., 2001).

Computed values for ΔGPE are in general negative (Fig. 4c), resulting in compressive potential stresses (Fig. 4d). The variation of ΔGPE as a function of surface heat flow and for a constant R_q is relatively complex: when increasing heat flow, ΔGPE first decreases significantly, becomes almost stationary and finally increases slightly. Predicted GPSt vary from −14 to 0 MPa as a function of surface and crustal heat flow. In detail, for R_q constant (e.g. $R_q = 40\%$, Fig. 4), potential stresses vary inversely to heat flow (i.e. the higher the heat flow the more compressive the stresses) or, alternatively, vary positively with lithosphere thickness. Fig. 5 shows that for lithospheres at sea level and with similar crustal thickness, the sign of the computed lithostatic pressure difference (i.e. $\sigma_{zz}(z) - \sigma^R{}_{zz}(z)$) switches from positive to negative at ~20 km depth and, for lithospheres thicker than ~150 km, switches again from negative to positive. Furthermore, the "positive lobe" below 150 km becomes larger when the base of the lithosphere deepens. Following Eq. (14) ΔGPE is equal to the algebraic sum of the areas limited by the function $\sigma_{zz}(z) - \sigma^R{}_{zz}(z)$ and Fig. 5 shows that the absolute values of ΔGPE and,

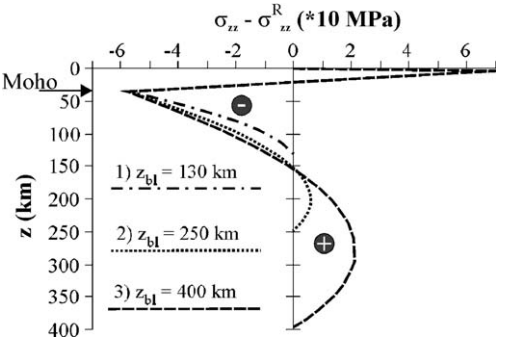

Fig. 5. Lithostatic pressure variation with depth between lithospheric columns and the asthenosphere reference column. Results for three distinct lithospheric columns with R_q ~40% but with contrasting thickness and surface heat flow: (1) $q_S = 60$ mW/m^2, (2) $q_S = 50$ mW/m^2 and (3) $q_S = 40$ mW/m^2. For each lithosphere column (e.g. column 3), ΔGPE is equal to the sum of the areas limited by the lithostatic pressure function (i.e. dashed line) and the vertical axis at the centre of the graph (see also Eq. (14)). The graph shows that as the base of the lithosphere deepens, the algebraic sum of the individual areas (i.e. ΔGPE) decreases. Crustal configuration and parameter values as in Fig. 4.

consequently, GPSt values tend to be lower for thicker lithospheres (i.e. $z_{bl}>150$ km). This result reflects the increase with depth of (1) asthenosphere density (i.e. Eq. (7)) and of (2) mantle lithosphere thermal expansivity (i.e. Eq. (6)), but also reflects the fact that thick lithospheres are associated with chemically depleted mantle roots (Jordan, 1978 and Fig. 4a and b). In summary, body forces for thick lithospheres tend to be more tensile, or less compressive, than for thinner ones. This is also valid if q_S is fixed and R_q is allowed to vary. For example, if $q_S=50$ mW/m^2 and R_q varies between 30% and 60%, z_{bl} deepens from ~140 km to ~390 km (Fig. 4a) and potential stresses decrease by 13 MPa (Fig. 4d).

3.2. Interplay between surface heat flow, topography and Moho topography

Topography is explored in the range of −500 to 1000 m, as topographies below −500 m are more typical of thinned passive margins and topographies above 1000 m are more likely to be supported by dynamic loads rather than by lithosphere buoyancy. Modelling results shown in Fig. 6 are for 35-km-thick crust and $R_q=40\%$.

In agreement with previous studies (e.g. Coblentz et al., 1994), submerged landmasses are, in general, submitted to compressive gravitational potential stresses whereas elevated ones are spontaneously under tension (Fig. 6). However, this first-order correlation is disturbed by the control that surface heat flow exerts on the thickness (Fig. 6a) and the density (Fig. 6b) of mantle lithosphere. The present results suggest that maximum ΔGPE due to changes in surface heat flow can be on the order of ~$2–7\cdot10^{12}$ N/m (Fig. 6c), resulting in GPSt variations up to ~16 MPa (Fig. 6d). Noteworthy, ΔGPE and GPSt gradients are more pronounced for very low heat flow values (i.e. $q_S<37$ mW/m^2), that are in the present case associated with lithospheres thicker than ~300 km. Fig. 6d shows, however, that potential stresses are more sensitive to crust elevation than to surface

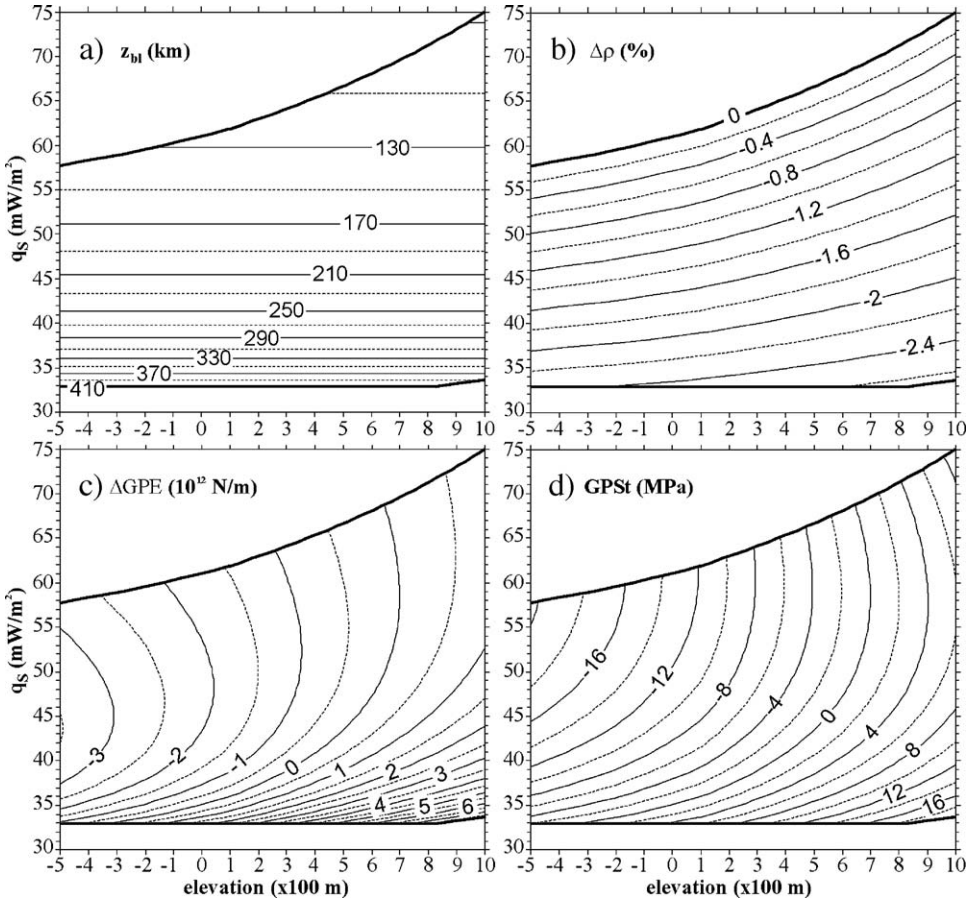

Fig. 6. Computed (a) base lithosphere depths (z_{bl}), (b) density depletion of mantle lithosphere with respect to the asthenosphere ($\Delta\rho$), (c) ΔGPE and (d) GPSt as a function of surface topography and surface heat flow (q_S). The crust is assumed to be 35 km thick, and $R_q=40\%$. Parameter values are given in Table 1.

heat flow. For example, for $q_S = 50$ mW/m^2 and for the range of elevations selected here, computed potential stresses vary from ~−18 to ~6 MPa. Even if the interval of possible elevations sustained by lithospheric buoyancy is reduced to the range [−500 m, +500 m], stress magnitudes still vary significantly by ~15 MPa.

Modelling results in function of surface heat flow and Moho topography for a crust exposed at sea level and $R_q = 40\%$ are shown in Fig. 7. Moho depth, or alternatively crustal thickness, was allowed to vary between 25 and 55 km in agreement with the global crustal thickness distribution compiled by Christensen and Mooney (1995). Values falling outside this range are usually characteristic of tectonically active regions which are not considered in the present paper.

The most unexpected result of Fig. 7 resides in the 'shark fin' shape of the solution domains. It suggests that very thick crust (i.e. more than 50 km thick) can be sustained by lithospheric buoyancy alone, only for a window of relatively low heat flow values. Thinner crust is associated with heat flow values outside this window and, in particular, to extremely low heat flow values. Although this result goes beyond the scope of the present contribution, it is interesting to note that it presents close similarities with the empirical relationship between lithosphere age (or alternatively surface heat flow) and crust thickness derived from a global seismic compilation by Durrheim and Mooney (1991, 1994), where Proterozoic crust was found to be extremely thick (i.e. 40 to 55 km) but Archean crust was found to be thinner (i.e. 27 to 40 km). We also note that extremely high heat flow values (i.e. $q_S > 75$ mW/m^2) are restricted to thin crust and mantle lithosphere.

ΔGPE and GPSt (Fig. 7c and d) are predicted to be far more sensitive to Moho topography than to surface topography or heat flow. Maximum variations in GPSt magnitudes as a function of Moho topography are in the order of ~60 MPa (i.e. for $q_S = 45$ mW/m^2). Therefore, tensile stresses produced by elevated surface topography can simply be cancelled out by the effect of deep Moho

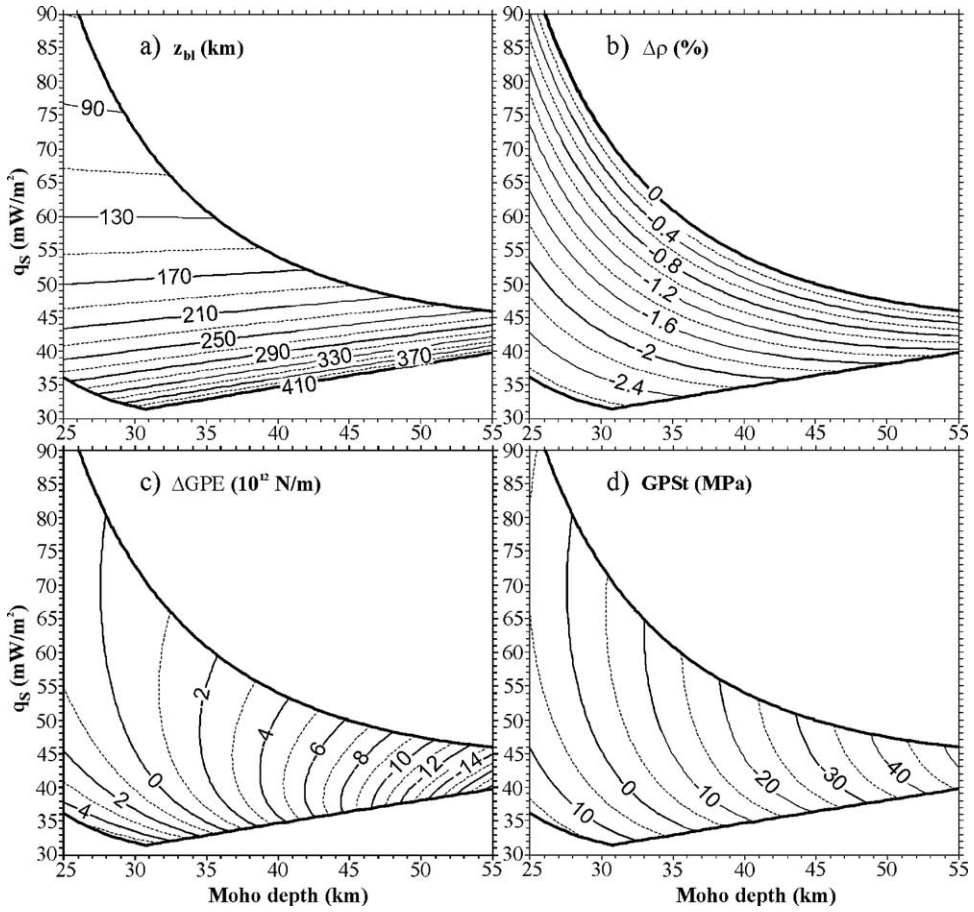

Fig. 7. Computed (a) base lithosphere depths (z_{bl}), (b) density depletion of mantle lithosphere with respect to the asthenosphere ($\Delta\rho$), (c) ΔGPE and (d) GPSt as a function of Moho depth and surface heat flow (q_S). Crustal surface at sea level and $R_q = 40\%$. Parameter values are given in Table 1.

topography as already noted by previous authors (Jones et al., 1996).

3.3. Interplay between surface heat flow and crust density

Since continental crust is heterogeneous in composition, its highly variable average density is prone to influence gravitational potential energy and stresses. In order to explore this influence, and its interplay with surface heat flow, different simulations were made by varying crustal density and surface heat flow for a 35-km-thick continental crust at sea level and R_q=40% (Fig. 8). The solution pattern suggests that lithospheres with relatively light crust (i.e. ρ_C<2750 kg/m^3) can be in local isostatic equilibrium only for low surface heat flow values (i.e. q_S<55 mW/m^2) and relatively thick lithospheres (i.e. z_{bl}>150 km, Fig. 8a). In contrast, lithospheres with a relatively dense crust (i.e. ρ_C>2900 kg/m^3) can be in isostatic equilibrium for a much wider range of heat flow values (Fig. 8). As shown previously, the solution pattern is also dependent on surface elevation and Moho depth, but elevating the crust would result in an upward shift of the upper boundaries (i.e. the $\Delta\rho$=0 contour in Fig. 8b) and the lower right boundaries (i.e. the $\Delta\rho$=2.65% contour in Fig. 8b) of the solution domains, whereas deepening the Moho would result in shifting these boundaries downwards. Consequently, the overall shape of the pattern of solutions remains when elevation and Moho depth vary.

As expected, ΔGPE and GPSt increase with crust density (Fig. 8c and d), resulting in tensional and compressional stress states for lithospheres with dense and light crusts, respectively. The present study suggests, however, that ΔGPE and GPSt are more sensitive to variations in crustal density than previously proposed by Coblentz et al. (1994). On average, for a 35-km-thick crust at sea level GPSt vary with 15 MPa for a ρ_C

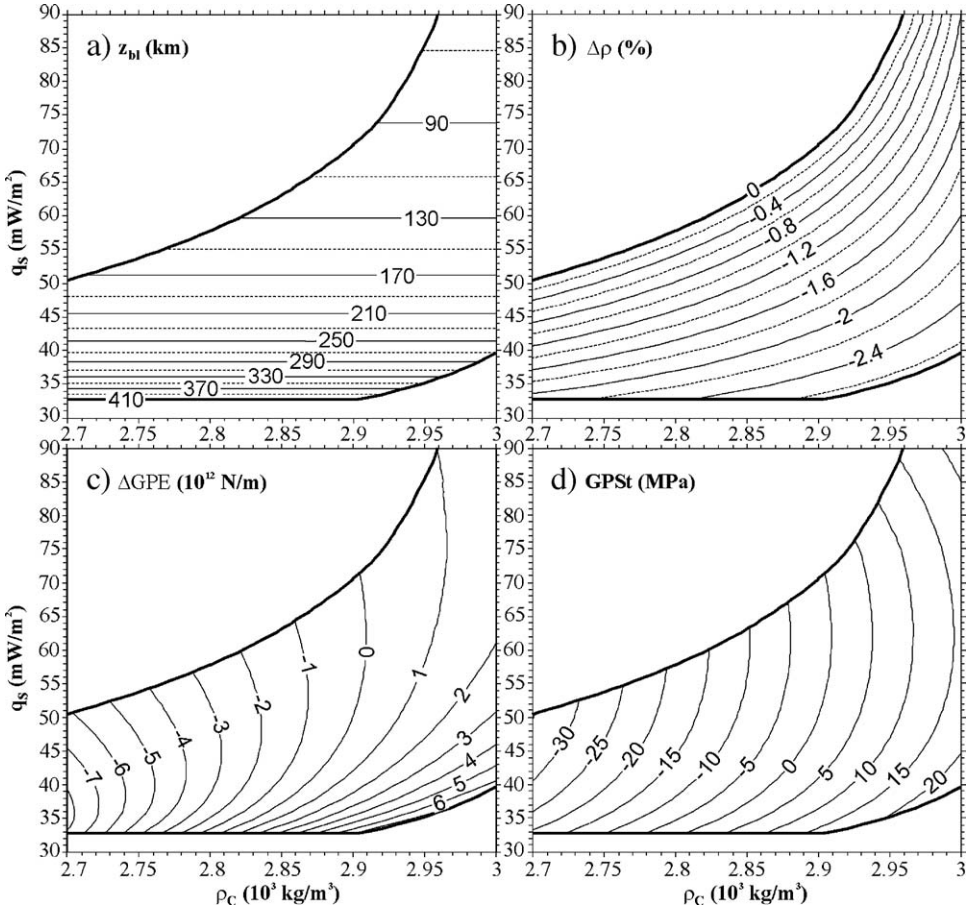

Fig. 8. Computed (a) base lithosphere depths (z_{bl}), (b) density depletion of mantle lithosphere with respect to the asthenosphere ($\Delta\rho$), (c) ΔGPE and (d) GPSt as a function of average crustal density and surface heat flow (q_S). The crust is assumed to be 35 km thick, its surface at sea level and R_q=40%. Parameter values are given in Table 1.

variation of 100 kg/m^3 (Fig. 8d). For a given crustal density value, potential stresses vary significantly by up to 10–15 MPa for the examined range of heat flow values (Fig. 8d). Noteworthy, for a constant ρ_C value, GPSt gradients are maximum when heat flow values are extremely low (i.e. q_S<35 mW/m^2). Even if these heat flow values that correspond to extremely thick lithospheres (i.e. z_{bl}>350 km, Fig. 8a) are excluded, GPSt still vary by 10 MPa.

4. Implications for the stress state of the Earth's lithosphere

In this section ΔGPE and GPSt are quantified for three continental lithosphere types with distinct tectonothermal ages: Archean, Proterozoic and Phanerozoic. The three continental lithosphere types are characterized by contrasting crustal thickness and densities (Durrheim and Mooney, 1991, 1994; Zoback and Mooney, 2003), but also by contrasting surface heat flow values (Pollack and Chapman, 1977; Nyblade and Pollack, 1993; Nyblade, 1999; Artemieva and Mooney, 2001). For comparison, results for oceanic lithosphere are also included here.

4.1. Archean lithosphere

Archean crustal thickness is assumed to be equal to 35 km, in agreement with results from a compilation of seismic experiments (Durrheim and Mooney, 1991, 1994). An average elevation of 450 m, typical for Precambrian cratons (Nyblade and Robinson, 1994), is selected. Surface heat flow is explored in the range of values commonly measured in Archean terrains, 30 to 50 mW/m^2 (Nyblade and Pollack, 1993). Base of lithosphere depths are now restricted to the range 190 to 370 km (Fig. 9a). This range encompasses most of previous determinations made by means of thermal modelling, seismic tomography, magnetotelluric soundings, and mantle xenolith studies for Archean cratons (see a review by Artemieva and Mooney, 2001). Furthermore, the deepest base of lithosphere value selected here has to be consistent with the observation of a flat and undisturbed 410 km discontinuity below cratons (Li et al., 1998; Chevrot et al., 1999; Niu et al., 2004). This observation implies that the base of the lithosphere has to be a few tens of km above the 410 km discontinuity (Niu et al., 2004). Finally, similar model runs not shown here for extreme base of lithosphere depths from 370 km to 410 km yielded unrealistically high mantle lithosphere depletion values. An average crustal density of 2830 kg/m^3 (Christensen and Mooney, 1995; Zoback and Mooney, 2003) is used. Other modelling parameters are listed in Table 1.

The predicted degree of density depletion for Archean mantle roots with respect to fertile asthenosphere ranges from −2.4% to −1.6% (Fig. 9b), corresponding to density values ranging from ~3309 to ~3336 kg/m^3. The lowest density values agree well with density determinations based on mean mineral compositions of Archean mantle xenoliths (i.e. 3310±16 kg/m^3, Poudjom Djomani et al., 2001; O'Reilly et al., 2001, and 3290 to 3310 kg/m^3, Pearson and Nowell, 2002), whereas the highest are in better agreement with density values obtained from coupled thermal-gravity models (Kaban et al., 2003).

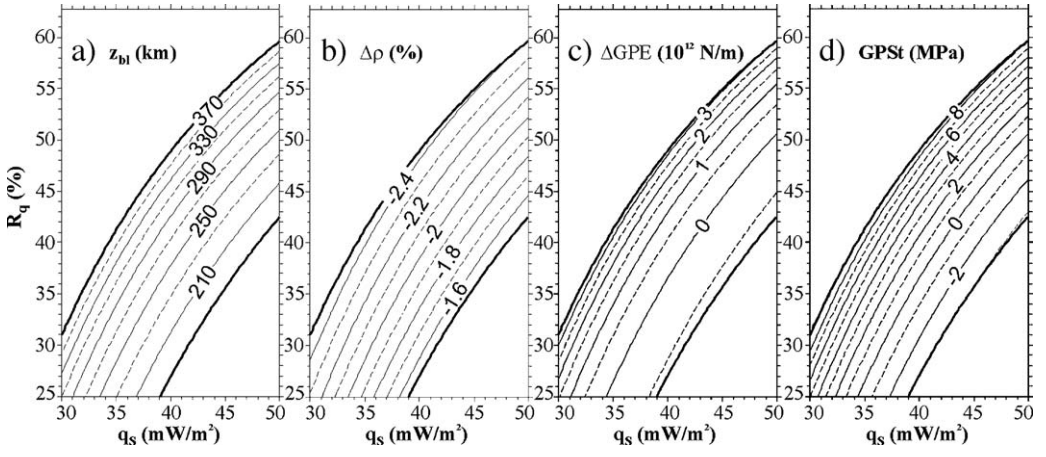

Fig. 9. Archean lithosphere. (a) Base lithosphere depths (z_{bl}), (b) density depletion of mantle lithosphere with respect to the asthenosphere ($\Delta\rho$), (c) ΔGPE and (d) GPSt as a function of surface heat flow (q_S) and R_q. Typical surface heat flow values for Archean terrains are explored here. Base lithosphere depth is assumed to be in between 190 km and 370 km. Elevation is 450 m, crustal thickness 35 km and average crustal density 2830 kg/m^3. Other parameters are given in Table 1.

The modelling results suggest that although ΔGPE can reach relatively high values, in particular for thick Archean lithospheres (i.e. up to $3 \cdot 10^{12}$ N/m in Fig. 9c), predicted GPSt magnitudes remain low and GPSt are in general tensile (Fig. 9d), in particular for $z_{bl} > \sim 230$ km (Fig. 9a).

4.2. Proterozoic lithosphere

In contrast to Archean crust, Proterozoic crust is in general characterized by a high velocity layer at its base (Durrheim and Mooney, 1991, 1994) resulting in a higher thickness and higher average density (Zoback and Mooney, 2003). For the calculations, an average thickness of 45 km (Durrheim and Mooney, 1994) and an average crustal density of 2880 kg/m^3 (Zoback and Mooney, 2003) were selected. Elevation is assumed to be equal to 450 m (i.e. average craton elevation, Nyblade and Robinson, 1994) and heat flow is allowed to vary between 40 and 60 mW/m^2 (Pollack and Chapman, 1977; Artemieva and Mooney, 2001). In agreement with previous estimates (e.g. Poudjom Djomani et al., 2001), modelled base of lithosphere depths are varied from 150 km to 250 km (Fig. 10a).

Proterozoic mantle lithosphere is predicted to be ~0.2% (i.e. $\rho_{MRef} \sim 3383$ kg/m^3) to ~1.4% (i.e. $\rho_{MRef} \sim 3342$ kg/m^3) lighter than asthenosphere (Fig. 10b). Although some relatively low depletion values are predicted for lithospheres thinner than ~170 km, this range of values is in good agreement with previous estimations based on thermal modelling (~0.6–0.7%, Artemieva and Mooney, 2001), gravity studies (1.1–1.5%, Kaban et al., 2003) and petrologic studies (~1.5%, Poudjom Djomani et al., 2001; Pearson and Nowell, 2002). Predicted ΔGPE values are negative (Fig. 10c) suggesting that Proterozoic lithosphere is spontaneously in a compressive state of stress. GPSt magnitudes are remarkably stable (i.e. vary less than 2 MPa, Fig. 10d) and relatively high throughout the solution domain.

4.3. Phanerozoic ("extended") lithosphere

Christensen and Mooney (1995) and Mooney et al. (1998) use the term "extended" to define Precambrian crust thinned in Phanerozoic times, regardless of potential reworking of the lithosphere by previous Phanerozoic orogenies. Although crustal accretion occurred in the Precambrian, it is commonly assumed that the last Phanerozoic thermo-tectonic (i.e. rift) event rejuvenated most of the lithosphere and in particular its mantle (e.g. Cloetingh et al., 1995). Consequently, this type of lithosphere is assumed to show similar characteristics as lithospheres formed during the Phanerozoic and, in the following, will be referred to as 'Phanerozoic lithosphere'. Phanerozoic crust is 30.5 km thick on average (Christensen and Mooney, 1995). Its average density is certainly lower than for Precambrian crusts, at least because its uppermost layer is made of a relatively thick pile of sediments. The empirical relationship between crustal thickness and average crustal density from Zoback and Mooney (2003) is used here. This relationship yields an average density of 2800 kg/m^3 for ~30-km-thick crust. A conservative value of +200 m is assumed for the elevation of Phanerozoic crust. Surface heat flow values are explored in the range 50 to 90 mW/m^2 (Pollack and Chapman, 1977; Chapman, 1986) and maximum base of lithosphere depth is fixed to 150 km (Fig. 11a).

Minimum base of lithosphere depth is limited to ~105 km by the imposed condition that $\Delta\rho = 0$. Thinner

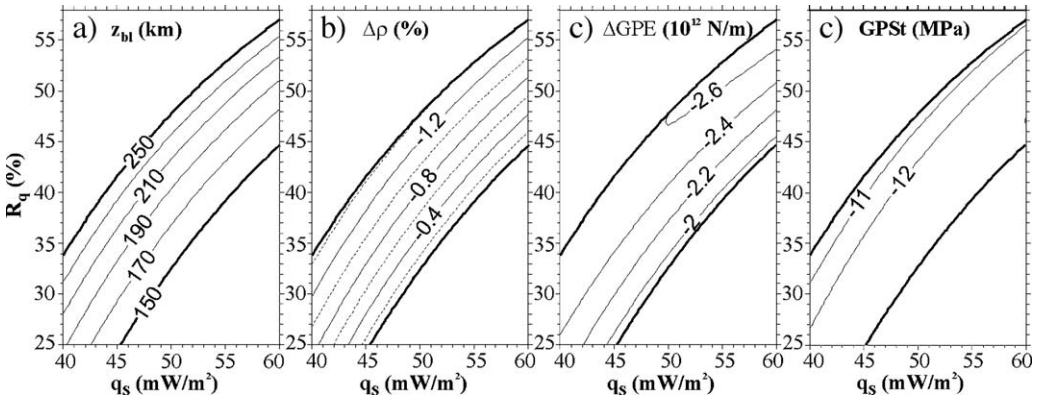

Fig. 10. Proterozoic lithosphere. (a) Base lithosphere depths (z_{bl}), (b) density depletion of mantle lithosphere with respect to the asthenosphere ($\Delta\rho$), (c) ΔGPE and (d) GPSt as a function of surface heat flow (q_S) and R_q. Typical surface heat flow values for Proterozoic terrains are explored here. Base lithosphere depth is varied from 150 km to 250 km. Elevation is 450 m, crustal thickness 45 km and crustal average density 2880 kg/m^3. Other parameters are given in Table 1.

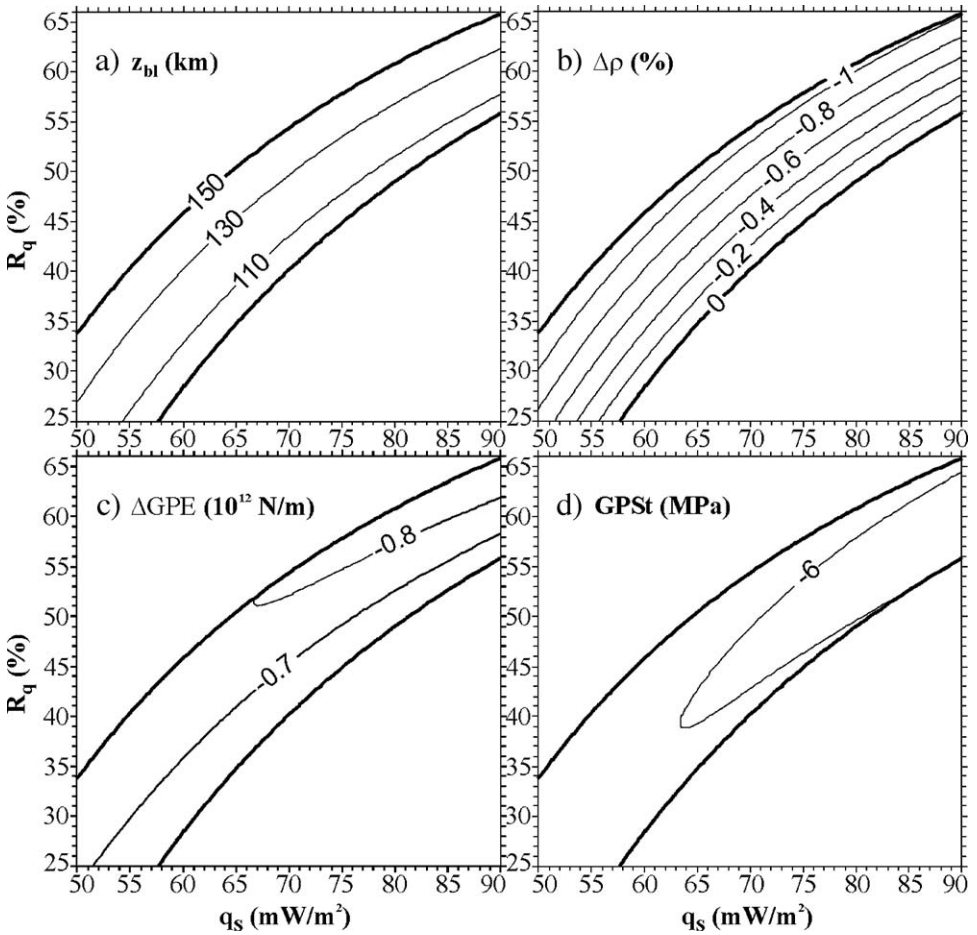

Fig. 11. Phanerozoic lithosphere. (a) Base lithosphere depths (z_{bl}), (b) density depletion of mantle lithosphere with respect to the asthenosphere ($\Delta\rho$), (c) ΔGPE and (d) GPSt as a function of surface heat flow (q_S) and R_q. Typical surface heat flow values for Phanerozoic terrains are explored here. Maximum base of lithosphere depth is fixed to 150 km. Elevation is 200 m, crust thickness 30.5 km and crust average density 2800 kg/m^3. Other parameters are given in Table 1.

Phanerozoic lithospheres could exist in the models, but only for mantle lithosphere reference density values higher than 3390 kg/m^3. Modelling results suggest that Phanerozoic mantle lithosphere is generally less depleted than its Precambrian counterparts (i.e. less than 1%, Fig. 11b). Noteworthy, depletion values corresponding to base of lithosphere depths between ~120 and 150 km (i.e. $\Delta\rho \sim 0.6$–1%) are in good agreement with results obtained from petrologic studies (Poudjom Djomani et al., 2001). Predicted ΔGPE values are negative and one order of magnitude less than ΔGPE values computed for Precambrian lithospheres (e.g. compare Fig. 11c with Fig. 10c). Integrated over the lithosphere thickness these values result in a mild compressive state (i.e. ~6 MPa, Fig. 11d) with a very constant magnitude (i.e. variations less than 1 MPa) over the whole range of parameter values explored here.

4.4. Oceanic lithosphere

In order to get a complete overview (Fig. 12), ΔGPE and GPSt variations from mid-oceanic ridges to old (i.e. >80 Ma) oceanic lithosphere are also computed. Elevation and heat flow values from Stein and Stein (1992) are used, assuming a 7-km-thick oceanic crust, ρ_{OC}=2850 kg/m^3 and a water column of 2.5 km above mid-oceanic ridges. Old oceanic lithosphere is predicted to be ~100 km thick, in agreement with previous estimates (e.g. Parsons and Sclater, 1977; Stein and Stein, 1992; Doin and Fleitout, 1996; McKenzie et al., 2005), and oceanic mantle lithosphere is predicted to be ~0.5% lighter than asthenosphere. This depletion value is probably the result of the combined effects of density depletion of the mantle due to melt extraction at mid-oceanic ridges (Oxburgh and Parmentier, 1977) and addition of fertile asthenosphere to

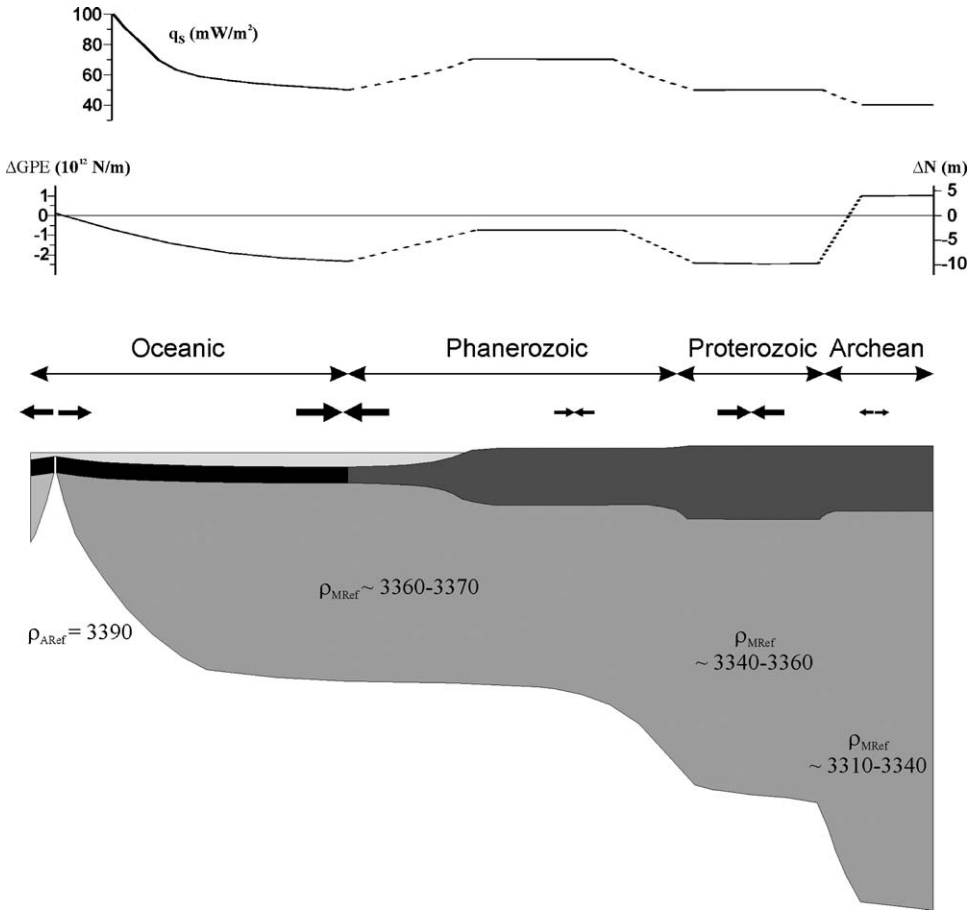

Fig. 12. Schematic cross-section of oceanic and continental lithospheres with distinct tectono-thermal ages, depicting conceptual relationships between elevation, crust thickness, surface heat flow, lithosphere thickness, chemical depletion of mantle lithosphere and gravitational potential energy (i.e. ΔGPE) and stresses (GPSt). Predicted geoid undulations originating in lateral changes in lithosphere structure (i.e. ΔN) were computed using Eq. (16). The width of the arrows suggests the magnitude of predicted GPSt.

the lithospheric column by conductive cooling (Parsons and Sclater, 1977). Variations in ΔGPE are shown in Fig. 12. The modelling predicts that mid-oceanic ridges are driven by tensional stresses with magnitudes by 16 MPa (i.e. $\Delta GPE = 0.11 \cdot 10^{-12}$ N/m for 7-km-thick lithosphere) whereas old oceanic basins are submitted to compressional stresses by −24 MPa (i.e. $\Delta GPE = -2.35 \cdot 10^{-12}$ N/m for 100-km-thick lithosphere). These stress magnitudes in old oceanic basins compare well with those proposed traditionally (e.g. Artyushkov, 1973; Dahlen, 1981; Fleitout and Froidevaux, 1983).

5. Discussion

Variations in gravitational potential energy and stresses for variations in lithosphere structure and age are shown in Fig. 12. These results are by nature first-order generalisations as they are derived from averaged relationships linking lithosphere age to the different parameters used in this study. As suggested by the analysis presented in the third section, departures of lithosphere properties from their inferred mean values can result in dramatic changes in ΔGPE and GPSt. Nevertheless, it is interesting to note that the predicted stress regimes are in good agreement with stress measurements compiled in the World Stress Map (Reinecker et al., 2005). This is especially true for oceanic lithosphere but also for most of the continental lithosphere where compressive stresses dominate (Reinecker et al., 2005). In detail, the modelling suggests higher compressive stresses in Proterozoic lithosphere than in Phanerozoic lithosphere. Archean lithosphere is predicted to be in slight extension. From existing stress measurements it is difficult to reject or confirm this latter result. If we exclude the anomalously elevated cratonic lithosphere of southern Africa only very few stress measurements from Archean terrains have been made public. It is worth

noting, however, that the predicted tensional GPSt could result from an underestimation of crustal thickness for Archean terrains. Increasing average crustal thickness values by 5 km would result in shifting GPSt values by −10 MPa (Fig. 7), leading to a slightly compressive state. We can, at least, conclude that Archean lithosphere is in a close to neutral stress state as already suggested by Doin et al. (1996).

This conclusion is in clear contradiction with results obtained by Zoback and Mooney (2003) who claim that lithospheres with thick and cold roots are dominated by very low ΔGPE values (i.e. down to $-15\cdot10^{12}$ N/m) and high compressive stresses. Although their work represents a substantial methodological improvement in the sense that realistic base lithosphere topographies were introduced in the modelling, these authors use too simplified mantle density distributions (i.e. constant densities) leading to unrealistic ΔGPE values, in particular in the case of thick lithospheres. The very low ΔGPE values computed by Zoback and Mooney (2003) would theoretically imply compressional stresses with magnitudes up to ~75 MPa and geoid lows with respect to mid-oceanic ridges down to −70 m. Such a strong correlation between geoid anomalies and cratons finds no support from gravity measurements (Jordan, 1988; Shapiro et al., 1999).

Published geoid analyses can be used to test the validity of the present results. Eq. (17) was used to compute geoid undulations caused by changes in lithosphere structure (Fig. 12). Geoid heights and lows are here referred to the chosen reference column (Fig. 2), but because variations in gravitational potential energy and in geoid height between this reference column and mid-oceanic ridges are small (i.e. $\Delta GPE=+0.11\cdot10^{12}$ N/m and $\Delta N=+0.5$ m, respectively), geoid undulations computed here can also be considered as referred to mid-oceanic ridges. Predicted geoid anomalies (i.e. $\Delta N=-10$ m for older than 80 Ma oceanic basins, Fig. 12) are in good agreement with observed anomalies (e.g. Haxby and Turcotte, 1978; Turcotte and McAdoo, 1979; Hager, 1983). Furthermore, computed geoid/age slopes (i.e. increasing from −0.17 m/Myr at 0–20 Ma to −0.04 at 80–100 Ma) fit reasonably well geoid slope data determined across transform faults (Richardson et al., 1995). Across passive margins, the geoid is predicted to jump with 6–7 m (Fig. 12) in agreement with values proposed by previous authors (Haxby and Turcotte, 1978; Doin et al., 1996). However, geoid variations across passive margins are expected to be very sensitive to variations in surface elevation and Moho depth in the continental domain (i.e. as sensitive as ΔGPE values are).

Geoid anomalies related to the density structure of the continental lithosphere are more difficult to extract. Doin et al. (1996) estimated differences in geoid height from −4 to +1 m for "stable" continental areas (i.e. Phanerozoic and Proterozoic platforms) and from −10 to 0 m for shields (i.e. Archean to Proterozoic) with respect to mid-ocean ridges. Shapiro et al. (1999) concluded that shield and platforms grouped together show geoid anomalies of −11±4 m. Despite the fact that the regionalisations made by Doin et al. (1996) and Shapiro et al. (1999) do not correspond strictly to those made in the present study, geoid anomalies computed here agree with these previous studies in (1) the amplitude of the signal (i.e. in the order of −1 to −10 m, Fig. 12) and (2) in the geoid/tectono-thermal age trend (i.e. the geoid drops with age). This latter rule is, however, predicted to break down in the case of Archean lithosphere (Fig. 12). Because available geoid analyses consider broad regions where the signals from Proterozoic and Archean lithospheres are mixed, as it is the case for predicted GPSt, it remains difficult to confirm or reject this modelling result.

The present study represents a step forward in quantifying gravitational potential energy using as much as possible realistic thermal and density structures for the lithosphere. However, further improvements of the method are still needed. These could involve, for example, the well-known temperature dependency of thermal conductivities but based on the recent study by McKenzie et al. (2005), we can anticipate that the present results will not be significantly affected by this latter refinement. Much care has to be taken when dealing with the assumption of simplified distribution of radioactive elements in the crust as it has been shown that more complex distributions might indeed characterize a large number of continental sections (Mareschal and Jaupart, 2004; Brady et al., 2006). Also, because the thermal adjustment time of thick lithospheres is similar to the timescale of radioactive decay, Michaut and Jaupart (2004) have recently questioned the thermal steady-state assumption for thick lithospheres. These authors advance cratonic mantle lithosphere temperatures up to 150 °C higher than those derived using a steady-state assumption. This implies mantle roots ~0.5% lighter than proposed here but does not affect significantly the results of the present paper.

Finally, it is worth noting that the simplified lithospheric model used here with a sharp lithosphere–asthenosphere boundary is an oversimplification of a system whose physics are still poorly known. The base of the lithosphere is merely not a sharp discontinuity but most probably a transition zone where small-scale convection occurs as suggested by Parsons and McKenzie (1978). Instabilities in this transition zone, caused for example by

drastic changes in lithosphere thickness (King and Anderson, 1998), would alter the steady-state thermal structure of the lithosphere (Cooper et al., 2004). Further and more advanced finite-element modelling work is required to test the influence of this eventual mechanism on the GPE state of the lithosphere.

6. Conclusions

In this study, it is shown that not only surface topography and crust density, but also surface heat flow, crustal heat flow and Moho depth have a significant impact on the net gravitational potential energy and potential stresses of the lithosphere. In particular, variations in the thickness of mantle roots, not taken into account in most previous studies, can result in dramatic changes in predicted potential stresses. The results presented here demonstrate that any attempt to estimate potential stresses from topography alone leads in most cases to erroneous results.

The present study also suggests that most of the stable continental lithosphere is, in general, in a spontaneous compressive stress state. Magnitudes associated with these compressive stresses are predicted to be higher in Proterozoic (i.e. ~12 MPa) than in Phanerozoic lithosphere (i.e. ~6 MPa). Archean lithosphere is found to be in a quasi neutral to slightly tensile stress state.

Acknowledgements

I am grateful for funding by NWO in the framework of the European Science Foundation Eurocores/Euromargins Programme (Nemsdyn-EMA16 Project). Susanne Buiter, Aline Saintot and two anonymous reviewers are acknowledged for valuable and constructive comments on an earlier version of the paper, other comments were made by Jean-Claude Mareschal and Marie-Pierre Doin. This is the Netherlands Research School of Sedimentary Geology (NSG) publication no. 20060602.

References

Artemieva, I.M., Mooney, W.D., 2001. Thermal thickness and evolution of Precambrian lithosphere: a global study. J. Geophys. Res. 106, 16387–16414.

Artyushkov, E.V., 1973. Stresses in the lithosphere caused by crustal thickness inhomogeneities. J. Geophys. Res. 78, 7675–7708.

Balling, N., 1995. Heat flow and thermal structure of the lithosphere across the Baltic Shield and the northern Tornquist Zone. Tectonophysics 244, 13–50.

Boyd, F.R., 1989. Compositional distinction between oceanic and cratonic lithosphere. Earth Planet. Sci. Lett. 96, 15–26.

Boyd, F.R., McCallister, R.H., 1976. Densities of fertile and sterile garnet peridotites. Geophys. Res. Lett. 3, 509–512.

Boyd, F.R., Pearson, D.G., Mertzman, S.A., 1999. Spinel-facies peridotites from the Kaapvaal root. In: Gurney, J.J., et al. (Ed.), Proceedings of the VIIth International Kimberlite Conference, vol. 1, pp. 40–48. Red Roof Design, Cape Town, South Africa.

Brady, R.J., Ducea, M.N., Kidder, S.B., Saleeby, J.B., 2006. The distribution of radiogenic heat production as a function of depth in the Sierra Nevada Batholith, California. Lithos 86, 229–244.

Chapman, D.S., 1986. Thermal gradients in the continental crust. In: Dawson, J.B., et al. (Ed.), The Nature of the Lower Continental Crust. Geological Society Special Publications, vol. 24. Geological Society of London, London, United Kingdom, pp. 63–70.

Chevrot, S., Vinnik, L., Montagner, J.-P., 1999. Global-scale analysis of the mantle Pds phases. J. Geophys. Res. 104, 20203–20219.

Christensen, N.J., Mooney, W.D., 1995. Seismic velocity structure and composition of the continental crust: a global view. J. Geophys. Res. 100, 9761–9788.

Cloetingh, S., van Wees, J.D., van der Beek, P.A., Spadini, G., 1995. Extension in convergent regimes: constrains from thermomechanical modelling of Alpine/Mediterranean basins and intracratonic rifts. Mar. Pet. Geol. 12, 793–808.

Coblentz, D.D., Richardson, R., Sandiford, M., 1994. On the gravitational potential of the Earth's lithosphere. Tectonics 13, 929–945.

Cooper, C.M., Lenardic, A., Moresi, L., 2004. The thermal structure of stable continental lithosphere within a dynamic mantle. Earth Planet. Sci. Lett. 222, 807–817.

Dahlen, F.A., 1981. Isostasy and the ambient state of stress in the oceanic lithosphere. J. Geophys. Res. 86, 7801–7807.

Doin, M.-P., Fleitout, L., 1996. Thermal evolution of the oceanic lithosphere: an alternative view. Earth Planet. Sci. Lett. 142, 121–136.

Doin, M.-P., Fleitout, L., McKenzie, D., 1996. Geoid anomalies and the structure of continental and oceanic lithospheres. J. Geophys. Res. 101, 16119–16135.

Durrheim, R.J., Mooney, W.D., 1991. Archean and Proterozoic crustal evolution: evidence from crustal seismology. Geology 19, 606–609.

Durrheim, R.J., Mooney, W.D., 1994. Evolution of Precambrian lithosphere: seismological and geochemical constraints. J. Geophys. Res. 99, 15359–15374.

England, P.C., Houseman, G.A., 1989. Extension during continental convergence, with application to the Tibetan Plateau. J. Geophys. Res. 94, 17561–17579.

Fleitout, L., Froidevaux, C., 1982. Tectonics and topography for a lithosphere containing density heterogeneities. Tectonics 1, 21–56.

Fleitout, L., Froidevaux, C., 1983. Tectonic stresses in the lithosphere. Tectonics 3, 315–334.

Guyot, F., Wang, Y., Gillet, P., Ricard, Y., 1996. Quasi-harmonic computations of thermodynamic parameters of olivines at high-pressure and high-temperature. A comparison with experiment data. Phys. Earth Planet. Inter. 98, 17–29.

Hager, B.H., 1983. Global isostatic geoid anomalies for plate and boundary layer models of the lithosphere. Earth Planet. Sci. Lett. 63, 97–109.

Haxby, W.F., Turcotte, D.L., 1978. On isostatic geoid anomalies. J. Geophys. Res. 83, 5473–5478.

James, D.E, Boyd, F.R., Schutt, D., Bell, D.R., Carlston, R.W., 2004. Xenolith constraints on seismic velocities in the upper mantle beneath southern Africa. Geochem. Geophys. Geosyst. 5, 1–32.

Jones, C.H., Unruh, J.R., Sonder, L.J., 1996. The role of gravitational potential energy in active deformation in the southwestern United States. Nature 381, 37–41.

Jordan, T.H., 1978. Composition and development of the continental tectosphere. Nature 274, 544–548.
Jordan, T.H., 1988. Structure and formation of the continental tectosphere. J. Petrol. 29, 11–37.
Kaban, M.K., Schwintzer, P., Artemieva, I.M., Mooney, W.D., 2003. Density of the continental roots: compositional and thermal contributions. Earth Planet. Sci. Lett. 209, 53–69.
King, S.D., Anderson, D.L., 1998. Edge driven convection. Earth Planet. Sci. Lett. 160, 289–296.
Kukkonen, I.T., Peltonen, P., 1999. Xenolith-controlled geotherm for the central Fennoscandian Shield: implications for lithosphere–asthenosphere relations. Tectonophysics 304, 301–315.
Lachenbruch, A.H., Morgan, P., 1990. Continental extension, magmatism and elevation; formal relations and rules of thumb. Tectonophysics 174, 39–62.
Li, A., Fischer, K.M., Wysession, M.E., Clarke, T.J., 1998. Mantle discontinuities and temperature under the North American continental keel. Nature 395, 160–163.
Lithgow-Bertelloni, C., Guynn, J.H., 2004. Origin of the lithospheric stress field. J. Geophys. Res. 109, doi:10.1029/2003JB002467.
Mareschal, J.C., Jaupart, C., 2004. Variations of surface heat flow and lithospheric thermal structure beneath the North American craton. Earth Planet. Sci. Lett. 223, 65–77.
McKenzie, D., Jackson, J., Priestley, K., 2005. Thermal structure of oceanic and continental lithosphere. Earth Planet. Sci. Lett. 233, 337–349.
Michaut, C., Jaupart, C., 2004. Nonequilibrium temperatures and cooling rates in thick continental lithosphere. Geophys. Res. Lett. 31, doi:10.1029/2004GL021092.
Mooney, W.D., Laske, G., Masters, T.G., 1998. Crust 5.1: A global crustal model at 5°×5°. J. Geophys. Res. 103, 727–747.
Niu, F., Levander, A., Cooper, C.M., Lee, C.-L.A., Lenardic, A., James, D.E., 2004. Seismic constraints on the depth and composition of the mantle keel beneath the Kapvaal craton. Earth Planet. Sci. Lett. 224, 337–346.
Nyblade, A.A., 1999. Heat flow and the structure of the Precambrian lithosphere. Lithos 48, 81–91.
Nyblade, A.A., Pollack, H.N., 1993. A global analysis of heat flow from Precambrian terrains: implications for the thermal structure of Archean and Proterozoic lithosphere. J. Geophys. Res. 98, 12207–12218.
Nyblade, A.A., Robinson, S.W., 1994. The African Superswell. Geophys. Res. Lett. 21, 765–768.
O'Reilly, S.Y., Griffin, W.L., Poudjom Djomani, Y.H., Morgan, P., 2001. Are lithospheres forever? Tracking changes in subcontinental lithospheric mantle through time. GSA Today 11, 4–10.
Oxburgh, E.R., Parmentier, E.M., 1977. Compositional and density stratification in oceanic lithosphere—causes and consequences. J. Geol. Soc. (Lond.) 133, 343–355.
Parsons, B., McKenzie, D., 1978. Mantle convection and the thermal structure of plates. J. Geophys. Res. 83, 4485–4496.
Parsons, B., Sclater, J.G., 1977. An analysis of the variation of ocean floor bathymetry and heat flow with age. J. Geophys. Res. 82, 803–827.
Pearson, D.G., Nowell, G.M., 2002. The continental lithosphere mantle: characteristics and significance as a mantle reservoir. Philos. Trans. R. Soc. Lond., A 360, 2383–2410.
Pollack, H.N., Chapman, D.S., 1977. On the regional variation of heat flow, geotherms, and lithospheric thickness. Tectonophysics 38, 279–296.
Poudjom Djomani, Y.H., O'Reilly, S.Y., Griffin, W.L., Morgan, P., 2001. The density structure of subcontinental lithosphere through time. Earth Planet. Sci. Lett. 184, 605–621.
Reinecker, J., Heidbach, O., Tingay, M., Sperner, B., Müller, B., 2005. The 2005 release of the World Stress Map (available online at www.world-stress-map.org).
Richardson, W.P., Stein, S., Stein, C.A., Zuber, M.T., 1995. Geoid data and thermal structure of the oceanic lithosphere. Geophys. Res. Lett. 14, 1913–1916.
Ringwood, A.E., 1975. Composition and Petrology of the Earth's Mantle. McGraw-Hill, New York. 619 pp.
Rudnick, R.L., McDonough, W.F., O'Connell, R.J., 1998. Thermal structure, thickness and composition of continental lithosphere. Chem. Geol. 145, 395–411.
Schulze, D.J., 1989. Constraints on the abundance of eclogite in the upper mantle. J. Geophys. Res. 94, 4205–4212.
Shapiro, S.S., Hager, B.H., Jordan, T.H., 1999. The continental tectosphere and Earth's long-wavelength gravity field. Lithos 48, 135–152.
Stein, C.A., Stein, S., 1992. A model for the global variation in oceanic depth and heat flow with lithospheric age. Nature 359, 123–129.
Thybo, H., Zhou, S., Perchu, E., 2000. Intraplate earthquakes and a seismically defined lateral transition in the upper mantle. Geophys. Res. Lett. 27, 3953–3956.
Turcotte, D.L., McAdoo, D.C., 1979. Geoid anomalies and the thickness of the lithosphere. J. Geophys. Res. 84 (B5), 2381–2387.
Turcotte, D.L., Schubert, G., 2002. Geodynamics, 2nd ed. Cambridge University Press. 456 pp.
Turcotte, D.L., Haxby, W.F., Ockendon, J.R., 1977. Lithospheric instabilities. In: Talwani, M., Pitman, W.C. (Eds.), Island arcs, deep sea trenches and back-arc basins. Maurice Ewing Series, vol. 1. AGU, Washington DC, USA, pp. 63–69.
Zoback, M.L., Mooney, W.D., 2003. Lithospheric buoyancy and continental intraplate stresses. Int. Geol. Rev. 45, 95–118.